Equilibrium interphase interfaces and premelting of the Pb(110) surface

A. Landa and P. Wynblatt
Materials Science and Engineering Department, Carnegie Mellon University, Pittsburgh, Pennsylvania 15213

H. Häkkinen,* R. N. Barnett, and Uzi Landman
School of Physics, Georgia Institute of Technology, Atlanta, Georgia 30332
(Received 19 October 1994)

Equilibrium properties of the solid-liquid and liquid-vapor interphase interfaces of lead and surface melting of Pb(110) were investigated using molecular-dynamics simulations, with the glue model used for a description of the many-body interatomic interactions. The bulk melting temperature was determined to be 619±5 K for the model. Structural, energetic, and transport properties across the solid-liquid interface change gradually from bulk solid to bulk liquid behavior over a transition region of 5–6 (110) layers. The surface region of Pb(110) starts to disorder via generation of vacancies in the temperature range 350 K $< T <$ 400 K. The onset of a quasiliquid surface region is observed around 520 K. The surface disordering process reflects the anisotropy of the (110) surface, being enhanced in the direction parallel to the close-packed rows. Analysis of the results in the framework of the Landau-Ginzburg theory of surface melting shows that the thickness of the interfacial quasiliquid region grows logarithmically for $T >$ 520 K, with a correlation length of 7.7 Å, in close agreement with experimental results.

I. INTRODUCTION

Surface premelting, which is the existence of a liquid (or quasiliquid) at the solid-vapor (sv) interface at temperatures and pressures below the normal phase boundary, is a phenomena which has been the subject of a number of experimental and theoretical investigations. The suggestion that melting nucleates at the surface of the solid and the idea of surface melting dates back to 1842 (when Michael Faraday entered his ideas about snow and ice in his diary; see Ref. 1), and has been since a subject of interest, relating the existence of thin-liquid films on solid surfaces at temperatures below the bulk melting point to the absence of superheating of solids[2] (see Ref. 3 in this context). Nevertheless, detailed experiments, satisfactory theoretical treatments, and realistic computer simulations of the microscopic atomic-scale mechanisms of surface melting became available only recently.[4–8]

Surface melting can be viewed as the wetting of the solid-vapor interface by the liquid (or quasiliquid; see the following) upon approaching the triple point.[4–8] We emphasize that from this perspective we treat melting as a thermal equilibrium phenomena (devoid of kinetic effects) distinguished from melting of a crystal surface following irradiation (by a short photon pulse or electron beam as in laser and electron surface annealing experiments), which is a nonequilibrium phenomenon.[9] We note, however, that the surface melt layer at the initial stages of the process should be regarded as a quasiliquid exhibiting structural, dynamical, and transport properties that are intermediate between those of the solid and the bulk liquid. It is the formation of the thin quasiliquid layer, whose thickness grows as the temperature approaches T_M, which one appropriately terms surface premelting.[4,5]

One of the interesting results of experimental studies of surface melting is the crystalline face anisotropy of the phenomenon.[10,11] Thus, while the open faces of certain fcc crystals [Pb(110), Al(110), and Cu(110)] exhibit surface melting as defined above,[4,5,8,10–13] the phenomenon is not observed for the close-packed surfaces[4,11,13,14] [Pb(111), Al(111), and Cu(111)]. These observations have been rationalized using a phenomenological Landau-Ginzburg formulation,[15–19] leading to a surface melting condition which relates the interfacial free energies of the three phases γ_{sv}, γ_{lv}, and γ_{sl}, corresponding to solid-vapor, liquid-vapor, and solid-liquid equilibria, respectively. The condition[4,5]

$$\gamma_{sv}^{(hkl)}-\gamma_{lv}^{(hkl)}-\gamma_{sl}^{(hkl)}\equiv\Delta\gamma^{(hkl)}>0 \tag{1}$$

expresses the energy balance when a dry solid surface is replaced by one wetted by a liquid layer. The larger $\Delta\gamma^{(hkl)}$ is, the greater the free-energy gain and thus the tendency for surface premelting (the dependence of the γ's on the crystalline face is explicitly noted). According to this condition the surface will remain dry (i.e., no premelting) when $\Delta\gamma<0$. We remark[5] that, strictly speaking, the interfacial free energies in Eq. (1) are not necessarily the same as the equilibrium values for infinitely thick liquid films (consequently the crystal-free dependence of $\gamma_{sl}^{(hkl)}$ and $\gamma_{lv}^{(hkl)}$ which refers to the quasiliquid as discussed above). However, as argued previously,[5] out-of-equilibrium values can be estimated by extrapolation of known (empirical or semiempirical) equilibrium values. This criterion has been used to explain the results for Pb(110), where good estimates of the interfacial free energies are available.

The first molecular-dynamics simulation of surface melting of a metal treated the Al(110) surface.[13(a)] Subsequent investigations, using many-body interaction potentials appropriate for the description of metals, were performed for various other metal surfaces.[8,11,20–22] These investigations provided evidence for disordering of the

(110) surface of fcc metals via a vacancy-adatom generation mechanism mediating the formation of an adatom layer.[8,11,13,20] Furthermore, analysis of the results of simulations for the Cu(110) surface[8] [see also Ref. 22 for a study of Au(110)], motivated by the Landau-Ginzburg theory of surface melting, showed that the thickness of the quasiliquid layer increases logarithmically with temperature upon approaching the bulk melting temperature.

In this paper we present results of molecular-dynamics (MD) simulations of surface melting of the Pb(110) surface, which has been the most widely experimentally studied system, since the first surface melting investigations, in 1985,[23] using medium-energy ion scattering (MEIS, usually $\sim$100-keV H^+ beams). These measurements include MEIS,[23,24] low-energy quasielastic ion scattering (LEQIS) with supersonic He atom beams in the range of 2.2–6.5 meV,[25] low-energy electron diffraction (LEED),[12,26,27] high-resolution LEED (HRLEED),[28] laser-induced surface disordering studied by time-resolved reflection high-energy electron diffraction (TRRHEED),[29] and spin-polarized LEED (SPLEED),[30] as well as studies of structural changes of the Pb(110) surface using x-ray photoelectron diffraction (XPD),[31] diffuse light scattering (DLS) or diffuse reflectivity,[32] crystal-growth morphological studies,[33,34] scanning tunneling microscopy (STM),[35] scanning electron microscopy (SEM),[27,34] x-ray reflectivity (XRS),[36] and work-function measurements.[27,34]

The paper is organized as follows. Pertinent details of the glue-model and of the simulation and analysis methods are described in Sec. II. Determination of the bulk melting temperature and properties of the equilibrium interphase interfaces (lv and sl) of lead are given in Sec. III. Results of MD simulations of the premelting of Pb(110), pertaining to the evolution of the energetics, structure, and dynamics of the system with temperature, are given in Sec. IV, as well as analysis in the spirit of the Landau-Ginzburg theory, yielding results in agreement with those obtained from experiments. We summarize our results in Sec. V.

II. METHOD

To describe the interatomic interactions we use the so-called glue model,[37] which is a semi-empirical model, where in the spirit of other embedding schemes [e.g., the embedded-atom method (EAM) (Ref. 38) and effective-medium theory (EMT) (Ref. 39)] the total potential energy of N atoms in an arbitrary arrangement $\{\mathbf{r}_i\}$, $i=1,\ldots,N$, is written as

$$E=\frac{1}{2}\sum_{i,j=1}^{N}{}' \phi(r_{ij})+\sum_{i=1}^{N} U(n_i) , \tag{2}$$

where $r_{ij}=|\mathbf{r}_i-\mathbf{r}_j|$, the primed summation denotes omission of terms with $i=j$, $\phi(r)$ is a short-ranged pair potential, and U is a many-body term depending on a local generalized coordination of atom i, defined as

$$n_i=\sum_j \rho(r_{ij}) , \tag{3}$$

where $\rho(r)$ is a short-ranged monotonically decreasing function. The scheme has been optimized for Pb using experimental data on cohesive, elastic, vibrational, thermal-expansion, and surface properties, and has been used rather successfully in several studies of lead clusters and the Pb(111) surface where the nonmelting of that surface was demonstrated.[40]

In our molecular-dynamics simulations we use a setup of the system, and a methodology similar to that developed in previous studies of equilibrium interphase interfaces[41] and surface melting.[8,20] The semi-infinite system is modeled via a slab of interacting dynamic atoms which, in addition, interact with several crystalline layers of a static substrate of fcc(110) geometry. Periodic boundary conditions are imposed only in directions parallel to the surface. Our system has 26 layers each containing 88 dynamic atoms (8×11 atoms in the [001] and $[1\bar{1}0]$ directions, respectively) positioned on top of four static layers, resulting in 2288 dynamic atoms (including the static substrate, 2640 in total). Slabs of this size have been shown to be sufficiently thick and large for a reliable description of disordering and premelting phenomena at fcc(110) metal surfaces up to T_M.[8,11,20,41] The lattice constant of the static substrate at each temperature studied was adjusted to the value obtained from independent zero-pressure simulations of bulk Pb [employing three-dimensional (3D) periodic boundary conditions and the Parrinello-Rahman constant-pressure technique[42]]. From bulk simulations we find that the glue model reproduces the experimental lattice constant at room temperature [4.95 Å (Ref. 43)] and predicts the thermal-expansion coefficient to be $\alpha(300\ \mathrm{K})=1.8\times10^{-5}\ \mathrm{K}^{-1}$ and $\alpha(500\ \mathrm{K})=2.5\times10^{-5}\ \mathrm{K}^{-1}$ [experimentally $\alpha(300\ \mathrm{K})=2.9\times10^{-5}\ \mathrm{K}^{-1}$ (Ref. 43)]. In this context we note that our focus in this paper is on the behavior of the Pb(110) surface at temperatures well above room temperature, where, as shown below, the model yields results in quantitative agreement with experiments.

In the first stage of the study (Sec. III) we investigated the equilibrium properties of the (110) solid-melt and melt-vacuum interfaces at the coexistence temperature T_M, which we interpret as the bulk melting point of Pb given by the glue model. To reach the liquid-solid coexistence we followed the procedure outlined previously in Refs. 8, 20, and 41. We set up the above-mentioned (110) slab with a lattice parameter corresponding to the zero-pressure bulk value at 620 K, and heated the system (by scaling the particles' velocities) well above the experimental bulk melting point of 601 K,[43] which results in melting nucleated at the free surface, propagating deeper into the sample. Subsequently we continued to adjust the energy content of the sample until about half of the dynamical layers were melted. We then allowed the system to evolve at a constant energy for a prolonged period of time (1.5 ns). By analyzing different data segments in that period we verified that the solid-liquid interface had reached its equilibrium location apart from fluctuations of approximately ±0.5 monolayers, induced by the fluctuations of the kinetic and potential energies inherent in our finite sample. The results in Sec. III are based on the analysis of data collected during the last 500 ps of the

1.5-ns constant energy run.

In the second stage of the study (Sec. IV) we performed systematic simulations in the range from room temperature up to the estimated bulk melting point to investigate the surface properties of the (110) slab. At each temperature the system was equilibrated during the first 30–60 ps of the run, followed by a 60–100-ps production period for collecting data (longer runs corresponding to higher temperatures). The sequence of equilibration and production phases was repeated 2–3 times to check that true equilibrium was achieved. Configurations at the end of equilibrium runs were utilized as an initial configuration for a higher-temperature run with appropriate scaling of the lattice parameter. In all simulations the equations of motion for atoms were integrated using a fifth-order predictor-corrector algorithm with a time step of 5 fs.

Integration of the equations of motion yields the phase-space trajectories for the system from which physical properties and their time evolution can be obtained. To facilitate the presentation of our results, we define,[8] for any property q_i which depends on the phase-space point $(\mathbf{r}_i,\mathbf{p}_i)$ of atom i located at z_i (where $z=0$ is set at the bottom of the dynamic slab and increases toward the surface), a local density (per unit length) of that property at z by

$$\hat{\rho}_q(z)=\frac{1}{\sqrt{2\pi}\sigma}\sum_i q_i \exp\left[\frac{-(z-z_i)^2}{2\sigma^2}\right] . \tag{4}$$

In our calculations a value of about 10% of the layer spacing $d_{(110)}=a/2\sqrt{2}$ is used for the Gaussian width parameter σ. This allows us to exhibit our results as continuous profiles in the z direction. The particle number density (per length) profiles $\rho(z)$ are obtained by letting $q_i=1$ in Eq. (4). Other properties are presented as per particle local densities

$$g(z)=\hat{\rho}_q(z)/\rho(z) . \tag{5}$$

Further analysis of the properties of our system includes characterization of the atomic order (via calculation of layer structure factors which are used as order parameters, and layer pair distribution functions), as well as diffusive properties of atoms in different layers. The structure factor is given by

$$S_l(\mathbf{g}_\alpha)=\frac{1}{n_l}\sum_{i\in l} e^{i\mathbf{g}_\alpha\cdot\mathbf{r}_i},\quad \alpha=1,2,3 , \tag{6}$$

where $\mathbf{g}_\alpha$ is the αth vector in the reciprocal lattice corresponding to our calculational cell, and n_l is the total number of atoms in layer l. The layer pair distribution function is defined as

$$p_l(r_\parallel)=\left\langle\frac{1}{n_l}\sum_{i,j\in l}'\frac{1}{2\pi r_\parallel}\delta(r_{ij,\parallel}-r_\parallel)\right\rangle , \tag{7}$$

where $r_{ij,\parallel}$ is the magnitude of the component of $\mathbf{r}_i$-$\mathbf{r}_j$ parallel to the surface plane, n_l is the instantaneous number of atoms in layer l, the $i=j$ term is omitted from the sum, and angular brackets denote averaging over time. Diffusion coefficients are obtained from

$$D_l=\lim_{t\to\infty}\frac{R_l^2(t)}{2n_d t} , \tag{8}$$

where n_d is the dimensionality in calculation of the mean-squared displacements

$$R_l^2(t)=\left\langle\frac{1}{n_l}\sum_{i\in l}[\mathbf{r}_i(t+\tau)-\mathbf{r}_i(\tau)]^2\right\rangle , \tag{9}$$

with the sum including atoms in layer l at time τ, and the angular brackets indicating averaging over time origins, τ (typically 10–50 time origins are used).

III. BULK MELTING TEMPERATURE AND EQUILIBRIUM INTERPHASE INTERFACES

In this section we briefly discuss the properties of the solid-liquid and liquid-vacuum interfaces at the coexistence temperature T_M. Since the general properties of solid-liquid and liquid-vacuum interfaces in fcc metals have already been extensively studied in previous simulations,[8,20,41] we concentrate here only on features pertinent to the present study.

As seen from the density [Fig. 1(a)] and potential-energy [Fig. 1(b)] profiles, the system exhibits two interfaces (solid liquid and liquid vacuum). The maxima in the density profile correspond to the layer positions in the solid part of the slab, which are the minima in the potential-energy profile. The temperature profile (not shown) is uniform throughout the slab, with an average temperature of $T_M=619\pm5$ K, which we take as the bulk melting point of Pb given by the glue model, in reasonable agreement with the experimental melting point of

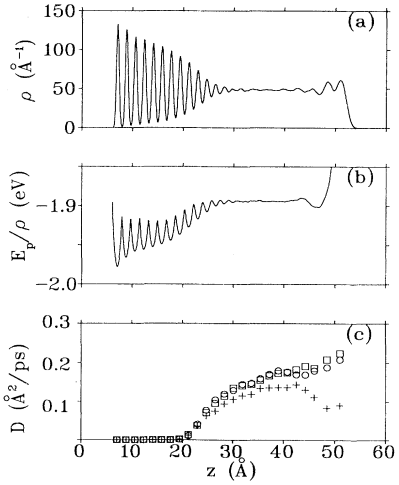

FIG. 1. Equilibrium profiles of the Pb(110) system at the bulk melting point vs distance z, normal to the (110) plane. (a) Density ρ, (b) per-particle potential energy E_p, and (c) diffusion coefficients in the [001] direction (squares), in the [1$\bar{1}$0] direction (circles), and in the [110] direction, normal to the surface (pluses). Energies and distances in eV and Å, respectively, and diffusion constants in Å^2/ps.

601 K.[43] We stress here that while estimates very close to ours have been given for glue Pb before,[40(b)] it is important to recheck the value of T_M, in the context of our premelting simulations, in order to analyze the growth behavior of the quasiliquid thickness in our sample reliably (see below). From the density and potential-energy profiles we estimate the density change across the solid-liquid interface, varying from $\rho_s = 0.032\,23$ Å^{-3} in the solid to $\rho_l = 0.031\,29$ Å^{-3} in the liquid (i.e., a decrease of 2.9%), and a latent heat of 0.058 ± 0.005 eV/atom, both in good agreement with the experimentally determined values of 3.5% for the density decrease of the solid upon melting[44] and 0.053 eV/atom for the latent heat,[45] respectively. We note in Fig. 1(c) that the diffusion in the bulk liquid region is isotropic in the x and y directions, with $D_x = D_y = 0.17 \pm 0.01$ Å^2/ps, in reasonable agreement with measurements of bulk liquid lead near T_M, $D = 0.22 \times 10^{-4}$ cm^2/s (Ref. 46) (Å^2/ps$= 10^{-4}$ cm^2/s). The fact that D_z remains smaller than D_x and D_y can be rationalized by considering the confined nature of the liquid in the z direction. This is particularly prominent at the liquid-vacuum interface, where we observe a strong layering effect combined with increased intralayer order [see Fig. 1(a)], as discussed below.

From the density and potential-energy profiles as well as the z dependence of the diffusion coefficients, we estimate that the transition region from solid ($z \lesssim 20$ Å in Fig. 1) to liquid extends over 5–6 atomic layers. A qualitative dynamic view of the solid-liquid interface is shown in Fig. 2. Viewing the system from the [1$\bar{1}$0] direction [Fig. 2(a)] we see a broadened and weakly faceted [atomic scale (111) facets] interface compared to a somewhat sharper interface viewed from the [001] direction [Fig. 2(b)]. This behavior, owing to the intrinsic geometry of the fcc(110) interface, has been discussed before in the context of MD simulations of the Cu(110) solid-liquid interface,[11] and is related to the relative free-energy difference of forming interfaces in (111) and (100) orientations. For those orientations it is energetically favorable to form relatively close-packed liquid layers on the liquid side of the interface, with the intralayer short-range order resembling that of the underlying solid side of the interface.[41] The slightly anisotropic structure of the interface seen in our simulations is similar to what was observed for the Cu(110) solid-liquid interface close to T_M,[8,11] but is much less pronounced than the structure of the interface in some other materials, particularly silicon, where the (001) sl interface exhibits atomically sharp (111) facets.[9,47]

Figure 3 shows the layer pair-distribution functions across the slab. These exhibit crystalline fcc(110) intralayer order for the bottom solid layers, changing gradually to conventional liquidlike behavior for the bulk liquid region, in accordance with previous simulations for other fcc metal systems using effective-medium and embedded-atom potentials.[8,11,20,41] In the present simulation we observe in addition a strong tendency toward densification and intralayer ordering of the two outermost liquid surface layers. While a certain degree of layering at the liquid-vapor interface has been observed in previous simulations[8,41] of Cu and Ni using EAM interactions, the effect is more pronounced in the current results for Pb. Accompanying the high degree of atomic packing in the liquid-to-vapor transition region, the position of the nearest-neighbor peak shifts from 3.5 Å in the solid layers to 3.2 Å in the two outermost liquid layers. The average number of atoms under the first and second maxima of $\rho(z)$ at the liquid surface is 146.1 and 150.5, respectively, and the peak-to-peak distance is 2.53 Å (as compared to about 88 atoms in a solid layer, with the spacing between solid layers being 1.76 Å). By visually inspecting snapshots of the two first layers of the liquid surface, recorded in our simulations, the intralayer ordering may be characterized as consisting of regions of (111) (hexagonal close packing) and (100) (packing in squares) types of order. The (100) type of ordering, particularly prominent for the outermost liquid layer, is further corroborated by the peak around 4.6 Å in the pair-distribution function for that layer. The ratio of the position of this peak to the position of the first peak at 3.2 Å is very close to $\sqrt{2}$, as expected for the intralayer (100) geometry. The tendency for mixed packing of (111) and

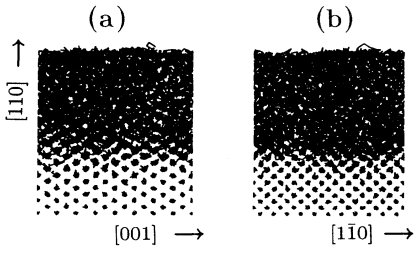

FIG. 2. Trajectories of atoms, projected onto the (1$\bar{1}$0) (a) and (001) (b) planes, over a time span of 10 ps at $T = T_M$. Note the broad and weakly faceted solid-liquid interface in (a), compared to a somewhat sharper interface in (b).

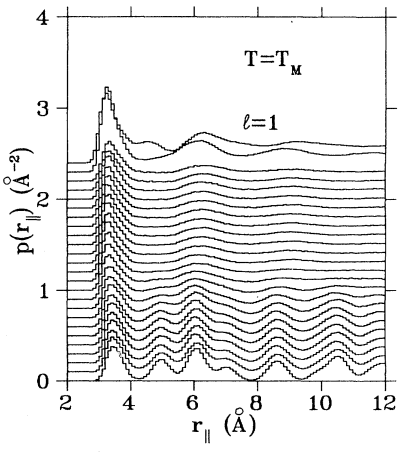

FIG. 3. Pair-distribution function $P(r_\parallel)$ for different layers at $T = T_M$. Note the prominent short-range order for the outermost liquid layer ($l = 1$, topmost curve) and the gradual change from solidlike to liquidlike order at the solid-liquid interface.

(100) types may be correlated with the fact that the glue model gives very similar surface formation energies for solid (111) and (100) surfaces (37.5 and 38.0 meV/Å^2, respectively[40(a)]). The embedded-atom and effective-medium interactions used in the previous simulations for Al(110), Ni(110), and Cu(110) surfaces[8,22,13,20] result in a larger relative difference between the surface energies of (111) and (100) geometries, and the (100) type of packing is lacking from the surface intralayer pair-distribution function in those simulations.

IV. SURFACE PREMELTING

To investigate variations of the properties of the system with temperature, we show first in Figs. 4–6 the density and potential-energy profiles of the system versus distance z normal to the surface plane, for various temperatures. From Fig. 4 we observe a gradual change of the density profile in the surface region with an increase in temperature, and the development of an adatom layer for $350 < T < 400$ K. By examining the position of the surface peaks in the $\rho(z)$ profiles in more detail, we find that at $T = 300$ K the surface layer relaxes inward, i.e., $\Delta_{12} = (d_{12} - d_{\text{bulk}})/d_{\text{bulk}} = -11.2\%$ [d_{12} is the distance between the topmost layer (1) and the second layer (2), and the spacing between (110) planes in the bulk is $d_{\text{bulk}} = a/2\sqrt{2}$]. At $T = 0$ we find $\Delta_{12} = -13.5\%$. These values are of comparable magnitude with experimental results,[48] where $\Delta_{12} = -15.9\%$ at $T = 0$ K and $\Delta_{12} = -14\%$ at 295 K.[49] The (incomplete) adlayer has a large inward relaxation, -36.3% at 400 K and -33.8% at 500 K, after which it merges into the peak in the density profile corresponding to the disordered surface layer (see Fig. 5), and the width of the disordered surface region begins to grow into the bulk. Consequently in the subsequent analysis for $T \geq 522$ K all atoms from the vacuum side of the interface up to the first minimum in $\rho(z)$ are assigned to the surface layer ($l = 1$).

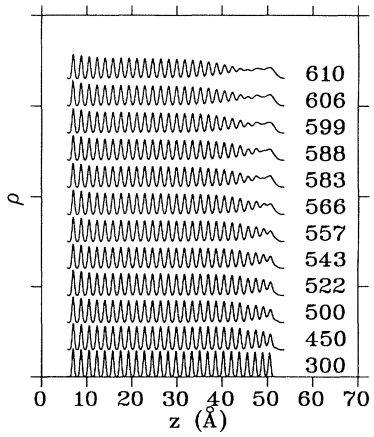

FIG. 4. Equilibrium density profiles $\rho(z)$ across the Pb(110) slab, normal to the (110) surface, for various temperatures. Distance in Å, density in Å^{-1}.

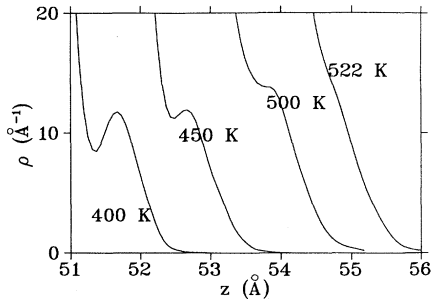

FIG. 5. Enlarged view of $\rho(z)$ at the surface, showing the density maximum corresponding to the adlayer merging into the surface layer ($l = 1$) peak around 520 K.

A gradual change with temperature is also observed in the per-particle potential-energy profiles shown in Fig. 6. For comparison we also include in Fig. 6 the per-particle potential-energy profile for the liquid-vacuum interface at the bulk melting point [from Fig. 1(b)]. We observe that at all temperatures the potential energy of atoms belonging to the first two surface layers ($l = 1$ and 2) is higher than that in deeper layers due to the reduced coordination in the surface region. For $T > 560$ K the potential energy for layers $l > 2$ also begins to increase, and at 610 K a surface region comprised of about five layers has a potential energy very close to the bulk liquid at $T_M = 619$ K.

The intralayer structure of the system is characterized via the calculated layer pair-distribution functions $p_l(r_\parallel)$ [Eq. (7)], shown in Fig. 7 for various temperatures 522 K $\leq T \leq$ 610 K. We note that around 520 K the long-range order in the surface layer begins to diminish,

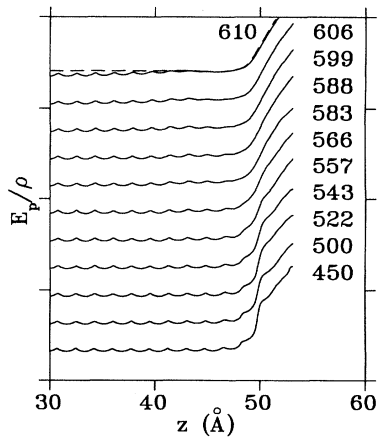

FIG. 6. Per-particle potential-energy profiles across the (110) slab, normal to the (110) surface, at various temperatures. The minima correspond to layer positions. The dashed curve corresponds to the potential-energy profile of the surface region of liquid Pb at $T = T_M$ [from Fig. 1(b)]. Energy in eV, distance in Å.

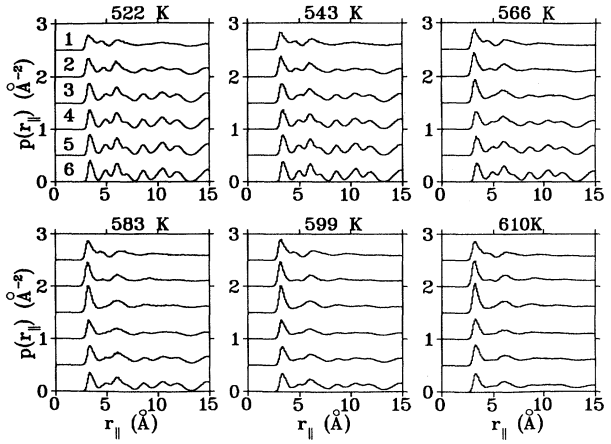

FIG. 7. Pair-distribution function $p(r_{\parallel})$ for the surface layers at temperatures indicated. Note the gradual disappearance of the long-range order as the temperature increases, starting from the surface layer ($l=1$), and the persistence of the short-range order in the surface layer at all temperatures.

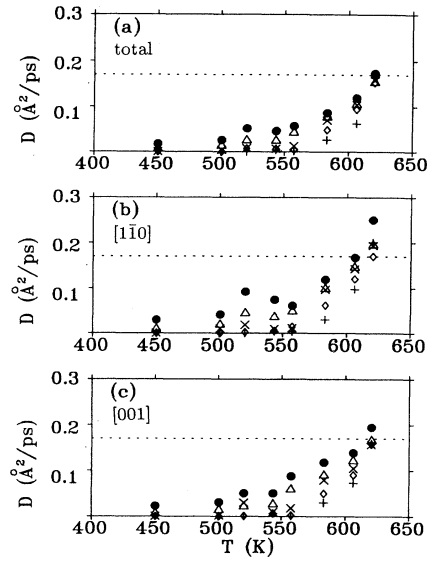

FIG. 8. Layer diffusion coefficients D_l as a function of temperature. Filled circles: $l=1$ (surface layer); triangles: $l=2$; crosses: $l=3$; diamonds: $l=4$; and pluses correspond to $l=5$. (a) Total D_l and (b) D_l along the close-packed rows ([1$\bar{1}$0] direction). (c) D_l across the ([001] direction) rows. Dotted line marks the calculated value of D in the bulk liquid at $T=T_M$. Note the slight anisotropy between [1$\bar{1}$0] and [001] directions in (b) and (c), and the marked increase of D_l for $l\geq 3$ at $T>560$ K. D_l in Å^0/ps, and temperature T in K.

reflected by the disappearance of the crystalline features in p_1 beyond 7.5 Å (i.e., $r>2d_{\mathrm{NN}}$, where d_{NN} is the nearest-neighbor distance). Between 522 and 610 K, the region showing liquidlike structure grows up to 5–6 layers. The gradual thickening of the liquidlike surface region, corroborated by Figs. 4, 6, and 7, is similar to what has been observed in previous simulations for other fcc(110) metal surfaces,[8,11,20] the only exception being that more short-range ($r<2d_{\mathrm{NN}}$) order is persistent for the first and second topmost surface layers for temperatures up to T_M.

The intralayer disordering of the surface region is accompanied by a rapid increase in the layer diffusion coefficients, shown in Fig. 8 versus temperature, calculated from the particle trajectories according to Eq. (8). The total diffusion coefficients [$n_d=3$ in Eq. (8)] for the topmost five layers are shown in Fig. 8(a), and a decomposition into diffusion coefficients in the [1$\bar{1}$0] and [001] directions is shown in Figs. 8(b) and 8(c), respectively. As is evident from the results, the layer diffusion coefficients for the first two surface layers begin to increase for $T>500$ K, with a marked increase for $l>2$ taking place for $T>560$ K. These observations correlate with the aforementioned structural variations at the surface region exhibited by the layer pair-distribution functions in Fig. 7 and the layer structure factors (see Fig. 9 and discussion below). We also note a marked anisotropy in diffusion between the two anisotropic directions of the Pb(110) surface in the early stages of the premelting (around 520 K $D_{[1\bar{1}0]}=1.8D_{[001]}$), and a slighter anisotropy for 560 K$<T<T_M$. [While some uncertainty is present because of the definition in Eq. (9), since atoms in a certain layer at time origin τ may make excursions from that region at later times, we estimate from our data that the influence of such events on our results is rather small at temperatures corresponding to the early stages of premelting and below, and is further alleviated by the averaging over time origins in Eq. (9).] This behavior agrees qualitatively with the He-scattering measurements of the diffusion at the premelted Pb(110) surface.[25(c)]

At first sight the decrease of $D_{[1\bar{1}0]}$ for 520 K $<T<560$ K seems surprising. However, it may be corre-

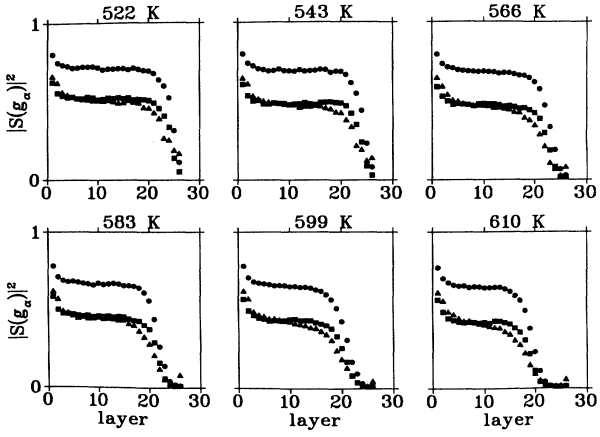

FIG. 9. Squared-layer-structure factors, $|S_l(\mathbf{g}_\alpha)|^2$, for $\alpha=1$, 2, and 3 (see text) denoted by squares, circles, and triangles, respectively, plotted vs layer number, at temperatures indicated.

lated with the decrease in the influence of the underlying solid substrate on the quasiliquid region as the solid-liquid interface moves deeper into the crystal, and with the densification and formation of the close-packed order in the surface layer of the quasiliquid.

Finally, we turn to a quantitative discussion of the temperature dependence of the order parameters and thickness of the quasiliquid. As mentioned in Sec. I, surface melting has been treated using the framework of the Landau-Ginzburg (LG) theory with single[15–19] and multicomponent[19] order parameters (OP's). A natural choice[8] for the order parameters $m(\mathbf{g}_\alpha,z)\equiv m(\alpha,z)$ are the squared magnitudes of the structure factors $|S_l(\mathbf{g}_\alpha,z)|^2$, calculated for each layer $1\le l\le N_L$ ($l=1$ and N_L denoting the surface layer and the dynamic layer next to the static substrate, respectively). The order-parameter profiles across the slab, calculated for various temperatures between 522 and 610 K, for $\mathbf{g}_1=(2\pi/a)(2,\bar{2},0)$, along the atomic rows, $\mathbf{g}_2=(2\pi/a)(0,0,2)$, across the rows, and $\mathbf{g}_3=(2\pi/a)(2,2,0)$, are shown in Fig. 9.

In the spirit of the LG theory we assume (see Ref. 8) the following form for the dependence of the order parameter on layer number [and thus distance along the normal to the (110) surface, increasing into the material]:

$$m_l(\alpha)=m_b+(\tilde{m}-m_b)e^{-\beta(l-l^*)}+(m_{ss}-m_b)e^{-\beta_{ss}(l_{ss}-l)},\quad l\ge l^*\ , \tag{10}$$

$$m_l(\alpha)=m^*e^{\gamma(l^*-l)},\quad l\le l^*\ , \tag{11}$$

where Eqs. (10) and (11) correspond to the solid and quasiliquid regions, respectively, and the model parameters depend on α, denoting the index of a reciprocal-lattice vector $\mathbf{g}_\alpha$. In our analysis we use $\mathbf{g}_1$ and $\mathbf{g}_2$, which lie along the $[1\bar{1}0]$ and [001] directions, i.e., along and across the close-packed rows of the (110) surface, respectively. The parameters β and γ are the OP decay factors in the solid and liquid regions, respectively, and l^* and m^* are the locations of the interface between the two regions and the value of the OP at the interface. m_b is the value of the OP in the bulk of the solid dynamical part of the system, and $\tilde{m}$ is a fitting parameter of the model. The quantities l_{ss}, m_{ss}, and β_{ss} denote the layer location of the interface between the static substrate and dynamic solid part of the system, an effective OP for the interface, and the decay factor into the dynamic solid, respectively.

Using the layers' structure factors $|S_l(g_\alpha)|^2$ obtained from the simulations at different temperatures, we minimize the function

$$F(m_b,\tilde{m},\beta,l^*,m_{ss},l_{ss}\beta_{ss})=\sum_{l=1}^{N_L}[m_l(\alpha)-|S_l(\mathbf{g}_\alpha)|^2]^2 \tag{12}$$

in the least-square sense. We find that in all cases the quality of the fit is such that $F/N_L\le 5\times10^{-5}$. As a result we show the position of the solid-quasiliquid interface as a function of temperature in Table I and Fig. 10, where we plot $l(T)$ (the number of liquidlike layers) as a function of $-\ln(1-T/T_M)$. A linear fit to $l(T)$ gives (l in monolayers)

TABLE I. Values of parameters obtained by least-squares fitting [see Eqs. (10)–(12)] using values for the structure factors for two reciprocal-lattice vectors ($\mathbf{g}_1$ and $\mathbf{g}_2$), obtained from simulations at various temperatures.

	$\mathbf{g}_1$				$\mathbf{g}_2$			
T (K)	m_b	m^*	l^*	β	m_b	m^*	l^*	β
610	0.428	0.157	6.7	0.584	0.654	0.261	6.2	0.511
606	0.434	0.136	5.2	0.449	0.652	0.237	5.1	0.502
599	0.441	0.182	5.1	0.486	0.661	0.262	4.7	0.435
588	0.449	0.174	4.0	0.609	0.663	0.308	4.0	0.629
583	0.464	0.166	4.0	0.561	0.671	0.309	4.2	0.645
566	0.473	0.174	2.9	0.549	0.682	0.277	2.7	0.526
557	0.487	0.150	1.8	0.582	0.693	0.255	1.7	0.509
543	0.487	0.201	1.8	0.719	0.695	0.257	1.1	0.609
522	0.522	0.186	1.2	0.638	0.712	0.261	0.8	0.636

$$l(T)=-(2.8\pm0.5)-(2.2\pm0.2)\ln(1-T/T_M),\quad (\mathbf{g}_1)\ , \tag{13}$$

$$l(T)=-(3.2\pm0.7)-(2.3\pm0.2)\ln(1-T/T_M),\quad (\mathbf{g}_2)\ . \tag{14}$$

We note that both $|S_l(\mathbf{g}_1)|^2$ and $|S_l(\mathbf{g}_2)|^2$ yield the same functional behavior for $l(T)$ within the accuracy of the fits.

In medium-energy ion-scattering (MEIS) (shadowing and blocking) experiments[24(d)] the backscattered ion yield is related to the number of positionally disordered atoms N (per surface area), reflecting the thickness of the disordered surface region. In Ref. 24(d) the behavior of N as a function of T was analyzed for $0.3\ \mathrm{K}\le T_M-T\le 40\ \mathrm{K}$ by fitting the data by the equation

$$N(T)=N_0\ln\left[\frac{T_M\Delta\gamma^{\mathrm{SR}}}{(T_M-T)N_0L}\right]\ , \tag{15}$$

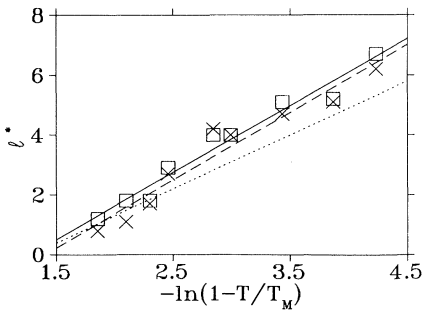

FIG. 10. The location of the solid-quasiliquid interface l^* (in monolayers) vs $-\ln(1-T/T_M)$, where $T_M=619$ K is the bulk melting point of Pb determined in our simulations. Squares and X's denote values obtained from the structure factor profiles calculated for $\mathbf{g}_1$ and $\mathbf{g}_2$, respectively, and solid and dashed lines show the corresponding linear fits. The dotted line is the result obtained from the MEIS experiment [see Ref. 24(d)].

where $\Delta\gamma^{SR}$ is the short-range contribution to the free energy of the solid-quasiliquid interface (dominating contribution at $T \leq T_M - 0.3$ K), L is the latent heat of melting, and N_0 is related to the correlation length within the liquid phase, ξ_{liq}. Defining $N(T) = l(T)\Delta z \rho_{liq}$, where $l(T)$ is the number of disordered (liquidlike) surface layers, and $N_0 = l_0 \Delta z \rho_l = \rho_{liq}\xi_{liq}/2$ [where ρ_{liq} is the particle number density of the liquid layer, and Δz is the (110) layer spacing], we can write Eq. (15) as

$$l(T) = \frac{\xi_{liq}}{2\Delta z} \ln \frac{\Delta\gamma^{SR}}{N_0 L} - \frac{\xi_{liq}}{2\Delta z} \ln(1 - T/T_M) \quad \text{(in ML)} , \tag{16}$$

corresponding to our Eqs. (13) and (14). By using the values quoted in Ref. 24(d) ($N_0 = 0.98 \times 10^{15}$ cm^{-2}, $\Delta\gamma^{SR} = 2.12$ mJ/m^2, $\xi_{liq} = 6.3$ Å, $\Delta z = 1.75$ Å, and $T_M = 600.7$ K) we find

$$l(T)_{exp} = -2.3 - 1.8 \ln(1 - T/T_M) , \tag{17}$$

which we also show in Fig. 10. In addition to establishing the logarithmic growth of the quasiliquid region, the result of our simulation follows closely the measured $l(T)_{exp}$, albeit with a slightly higher growth rate and thus larger correlation length (from our simulations $\xi_{liq} \approx 7.7$ Å as compared to[24(d)] $\xi_{liq,exp} \approx 6.3$ Å).

V. SUMMARY

Using molecular-dynamics simulations, with the glue model describing the many-body interatomic interactions, we have investigated the melting of the Pb(110) surface, as well as the properties of the (110) solid-to-liquid and liquid-to-vacuum interfaces of lead at the coexistence (bulk melting) temperature, which we determine from our simulations to be $T_M = 619 \pm 5$ K.

As in the case of previous studies of nickel[20,41] and copper[8,11] using embedded-atom and effective-medium interactions, the structural, energetic, and transport properties across the solid-liquid interface change gradually from bulk solid to bulk liquid behavior over a transition region of 5–6 (110) layers. The dynamic structure of the interface exhibits fluctuating atomic-scale (111) facets.

The surface region of Pb(110) starts to disorder via generation of vacancies and formation of an adlayer in the temperature range $350 < T < 400$ K. Around 520 K, we observe the onset of a quasiliquid surface region, exhibiting liquidlike energetic, structural, and transport properties. The disordering is enhanced in the direction parallel to the close-packed rows ([1$\bar{1}$0] direction), reflecting the anisotropic structure of the Pb(110) surface. While having lost the long-range order, the outermost layer of the quasiliquid retains a considerable amount of short-range order and shows a strong tendency to densification. The short-range order, also present at the liquid surface at $T = T_M$, can be characterized as consisting of areas of both (111) (hexagonal) and (100) (squarelike) types of close packing.

Analysis of our results within the framework of the Landau-Ginzburg theory shows that the thickness of the surface quasiliquid grows logarithmically for $T > 520$ K, in close correspondence with the well-established experimental data, with a slightly larger correlation length (7.7 Å) compared to the value (6.3 Å) inferred from the MEIS experiments.[24(d)]

ACKNOWLEDGMENTS

A.L. and P.W. acknowledge support by the National Science Foundation, Grant No. DMR90249776. The research of H.H., R.N.B., and U.L. is supported by the U.S. Department of Energy under Grant No. DE FG05-86ER45234 and the Air Force Office of Scientific Research, AFOSR Grant No. F49620-39-1-0231. Partial support for H.H. by the Academy of Finland is gratefully acknowledged. A.L. wishes to thank Dr. S. Foiles and Dr. F. Ercolessi for helpful discussions. Calculations have been performed on Cray Computers at the Pittsburgh Supercomputing Center under Grant No. DMR930031P, and the GIT Center for Computational Materials Science.

*Permanent address: Department of Physics, University of Jyväskylä, 40351 Jyväskylä, Finland.

[1]M. Faraday, *Lecture Before the Royal Institution* (1850) reported in *The Athenaeum* 1181, 640 (1933); Proc. R. Soc. London **10**, 440 (1860); *Faraday Diary* (Bell, London, 1933), Vol. II, pp. 79–81; see also W. A. Weyl, J. Colloid. Sci. **6**, 389 (1951).

[2]G. Tammann, Z. Phys. Chem. **68**, 205 (1910); Z. Phys. **11**, 609 (1910); I. N. Stranski, Die Naturwissenschaften **28**, 425 (1942); J. Frenkel, *Kinetic Theory of Liquids* (Oxford University Press, New York, 1946).

[3]H. Hakkinen and U. Landman, Phys. Rev. Lett. **71**, 1023 (1993), and references to experimental work on superheating of lead surfaces cited therein.

[4]See the review by J. van der Veen, B. Pluis, and A. W. Denier van der Gon, in *Chemistry and Physics of Solid Surfaces VII*, edited by R. Vanselow and R. F. Howe, Springer Series in Surface Science Vol. 10 (Springer-Verlag, Berlin, 1988), p. 455.

[5]J. F. van der Veen, B. Pluis, and A. W. Denier van der Gon, in *Kinetics of Ordering at Surfaces*, edited by M. G. Lagally (Plenum, New York, 1990), p. 343.

[6]J. G. Dash, in *Proceedings of the Solvay Conference on Surface Science: Austin, Texas, 1987*, edited by F. W. de Wette, Springer Series in Surface Science Vol. 14 (Springer-Verlag, New York, 1988), p. 142; in *Phase Transitions in Surface Films 2*, edited by H. Taub *et al.* (Plenum, New York, 1991), p. 339.

[7]H. Lowen, Phys. Rep. **237**, 249 (1994).

[8]R. N. Barnett and U. Landman, Phys. Rev. B **44**, 3226 (1991), and references therein.

[9]See U. Landman, W. D. Luedtke, M. W. Ribarsky, R. N. Barnett, and C. L. Cleveland, Phys. Rev. B **37**, 4637 (1988), and references therein.

[10]B. Pluis, T. N. Taylor, D. Frenkel, and J. F. van der Veen,

Phys. Rev. B **40**, 1353 (1989).
[11]H. Hakkinen and M. Manninen, Phys. Rev. B **46**, 1725 (1992), and references therein.
[12]P. von Blanckenhagen, W. Schommers, and V. Voegele, J. Vac. Sci. Technol. A **5**, 649 (1987).
[13](a) P. Stoltze, J. K. Norskov, and U. Landman, Phys. Rev. Lett. **61**, 440 (1988); (b) Surf. Sci. **220**, L693 (1989); P. Stoltze, J. Chem. Phys. **92**, 6306 (1990).
[14]A. W. Denier van der Gon, R. J. Smith, J. M. Gay, D. J. O'Connor, and J. F. van der Veen, Surf. Sci. **227**, 143 (1990).
[15]J. F. van der Veen, B. Pluis, and A. W. Denier van der Gon, *Kinetics of Ordering at Surfaces* (Ref. 5).
[16]R. Lipowsky, Phys. Rev. Lett. **49**, 1575 (1982).
[17]R. Lipowsky and W. Speth, Phys. Rev. B **28**, 3983 (1983).
[18]R. Lipowsky, Ferroelectrics **73**, 69 (1987).
[19]R. Lipowsky, U. Breuer, K. C. Prince, and H. P. Bonzel, Phys. Rev. Lett. **62**, 913 (1989); **64**, 2105 (1990); H. Lowen, *ibid.* **64**, 2104 (1990).
[20]E. T. Chen, R. N. Barnett, and U. Landman, Phys. Rev. B **41**, 439 (1990).
[21]P. D. Ditlevsen, P. Stoltze, and J. K. Norskov, Phys. Rev. B **44**, 13 002 (1991).
[22]F. Ercolessi, S. Iarlori, O. Tomagnini, E. Tosatti, and X. J. Chen, Surf. Sci. **251/252**, 645 (1991).
[23]J. W. M. Frenken and J. F. van der Veen, Phys. Rev. Lett. **54**, 134 (1985).
[24](a) J. W. M. Frenken, P. M. J. Maree, and F. van der Veen, Phys. Rev. B **34**, 7506 (1986); (b) B. Pluis, A. W. Denier van der Gon, and J. F. van der Veen, Surf. Sci. **239**, 265 (1990); (c) H. M. van Pinxteren, B. Pluis, and J. W. M. Frenken, Phys. Rev. B **49**, 13 798 (1994); (d) B. Pluis, T. N. Taylor, D. Frenken, and J. F. van der Veen, *ibid.* **40**, 1353 (1989).
[25](a) J. W. M. Frenken, J. P. Toennies, and Ch. Woll., Phys. Rev. Lett. **60**, 1727 (1988); (b) J. W. M. Frenken, J. Vac. Sci. Technol. A **7**, 2147 (1987); (c) J. W. M. Frenken, B. J. Hinch, J. P. Toennies, and Ch. Woll, Phys. Rev. B **41**, 938 (1990).
[26]K. C. Prience, U. Breuer, and H. P. Bonzel, Phys. Rev. Lett. **60**, 1146 (1988); U. Breuer, H. P. Bonzel, K. C. Prience, and R. Lipowsky, Surf. Sci. **223**, 258 (1989).
[27]A. Pavlovska and E. Bauer, Europhys. Lett. **9**, 797 (1989).
[28]H. N. Yang, T.-M. Lu, and G.-C. Wang, Phys. Rev. Lett. **63**, 1621 (1989); Phys. Rev. B **43**, 4714 (1991).
[29]J. W. Herman and H. E. Elsayed-Ali, Phys. Rev. Lett. **68**, 2952 (1992); Phys. Rev. B **49**, 4886 (1994).
[30]W. Durr, D. Pescia, J. Krewer, and W. Gudat, Solid State Commun. **73**, 119 (1990).
[31]U. Breuer, O. Knauff, and H. P. Bonzel, J. Vac. Sci. Technol. A **8**, 2489 (1990); Phys. Rev. B **41**, 10 848 (1990).
[32]H. N. Yang, K. Fang, T.-M. Lu, and G.-C. Wang, Phys. Rev. B **47**, 15 842 (1993); A. Pavlovska, H. Stephen, and E. Bauer, Surf. Sci. **234**, 143 (1990).
[33]J. C. Leyraud and J. J. Metois, J. Cryst. Growth **82**, 269 (1987); J. J. Metois and J. C. Heyraud, Ultramicroscopy **31**, 73 (1989).
[34]A. Pavlovska and E. Bauer, Appl. Phys. A **51**, 172 (1990).
[35]L. Kuipers and J. W. M. Frenken, Phys. Rev. Lett. **70**, 3907 (1993); J. W. M. Frenken, H. M. Pinxteren, and L. Kuipers, Surf. Sci. **283**, 283 (1993).
[36]B. Pluis, J. M. Gay, J. W. M. Frenken, S. Gierlotka, J. F. van der Veen, J. E. Macdonald, A. A. Williams, N. Piggins, and J. Als-Nielsen, Surf. Sci. **222**, L845 (1989).
[37]F. Ercolessi, M. Parrinello, and E. Tosatti, Philos. Mag. A **58**, 213 (1988).
[38](a) M. S. Daw and M. I. Baskes, Phys. Rev. B **29**, 6443 (1984); (b) S. M. Foiles, M. I. Baskes, and M. S. Daw, *ibid.* **33**, 7983 (1986).
[39]K. W. Jacobson, J. K. Norskov, and M. J. Puska, Phys. Rev. B **35**, 7423 (1987).
[40](a) H. S. Lim, C. K. Ong, and F. Ercolessi, Surf. Sci. **269/270**, 1109 (1992); (b) H. S. Lim, C. K. Ong, and F. Ercolessi, Z. Phys. D **26**, S45 (1993); (c) G. Bilalbegović, F. Ercolessi, and E. Tosatti, Euro. Phys. Lett. **17**, 333 (1992); **18**, 168 (1992).
[41]E. T. Chen, R. N. Barnett, and U. Landman, Phys. Rev. B **40**, 924 (1989).
[42]M. Parinello and A. Rahman, Phys. Rev. Lett. **45**, 1196 (1980).
[43]N. W. Ashcroft and N. D. Mermin, *Solid State Physics* (Saunders College, Philadelphia, 1976).
[44]T. E. Faber, *Introduction to the Theory of Liquid Metals* (Cambridge University Press, Cambridge, 1972).
[45]*Handbook of Chemistry and Physics,* edited by R. C. Weast (CRC, Cleveland, 1974).
[46]N. H. Nachtrieb, Ber. Bunsenges Phys. Chem. **80**, 678 (1976).
[47]U. Landman, W. D. Luedtke, R. N. Barnett, C. L. Cleveland, M. W. Ribarsky, E. Arnold, S. Ramesh, H. Baumgart, A. Martinez, and B. Khan, Phys. Rev. Lett. **56**, 155 (1986).
[48]J. W. M. Frenken, J. F. van der Veen, R. N. Barnett, U. Landman, and C. L. Cleveland, Surf. Sci. **172**, 319 (1986).
[49]J. W. M. Frenken, F. Huussen, and J. F. van der Veen, Phys. Rev. Lett. **58**, 401 (1987); B. Pluis, J. W. M. Frenken, and J. F. van der Veen, Phys. Scr. **19**, 382 (1987).